



Universiteit  
Leiden  
The Netherlands

## **Role of integrin adhesions in cellular mechanotransduction**

Balcioğlu, H.E.

### **Citation**

Balcioğlu, H. E. (2016, March 8). *Role of integrin adhesions in cellular mechanotransduction*. Retrieved from <https://hdl.handle.net/1887/38405>

Version: Corrected Publisher's Version

License: [Licence agreement concerning inclusion of doctoral thesis in the Institutional Repository of the University of Leiden](#)

Downloaded from: <https://hdl.handle.net/1887/38405>

**Note:** To cite this publication please use the final published version (if applicable).

Cover Page



Universiteit Leiden



The handle <http://hdl.handle.net/1887/38405> holds various files of this Leiden University dissertation

**Author:** Balcioğlu, Hayri Emrah

**Title:** Role of integrin adhesions in cellular mechanotransduction

**Issue Date:** 2016-03-08

## CHAPTER 2

---

# TUMOR-INDUCED REMOTE ECM NETWORK ORIENTATION STEERS ANGIOGENESIS <sup>1</sup>

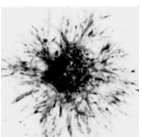
---

---

<sup>1</sup>This chapter is based on: Hayri E Balcioğlu, Bob vd Water and Erik HJ Danden, Tumor-induced remote ECM network orientation steers angiogenesis. *submitted: Scientific Reports*

## Abstract

Tumor angiogenesis promotes tumor growth and metastasis. Here, we use automated sequential microprinting of tumor and endothelial cells in extracellular matrix (ECM) scaffolds to study its mechanical aspects. Quantitative reflection microscopy shows that tumor spheroids induce radial orientation of the surrounding collagen fiber network up to a distance of five times their radius. Across a panel of  $\sim 20$  different human tumor cell lines, remote collagen orientation is correlated with local tumor cell migration behavior. Tumor induced collagen orientation requires contractility but is remarkably resistant to depletion of collagen-binding integrins. Microvascular endothelial cells undergo directional migration towards tumor spheroids once they are within the tumor-oriented collagen fiber network. Laser ablation experiments indicate that an intact physical connection of the oriented network with the tumor spheroid is required for mechanical sensing by the endothelial cells. Together our findings show that remote physical manipulation of the ECM network by the tumor steers angiogenesis.



## 2.1 Introduction

Tumor-associated angiogenesis is one of the hallmarks of cancer [1, 2]. The chemotactic aspect of this pathology has been well studied. Oncogenic signaling pathways and hypoxia occurring in tumors activate the release of growth factors, such as vascular endothelial growth factor (VEGF), which triggers the formation of new microvascular sprouts from pre-existing vessels. Inhibitors against this paracrine interaction, targeting mainly the VEGF receptor (VEGFR) on endothelial cells, have entered the clinic [3, 4].

Angiogenesis involves proliferation and migration of endothelial cells [5]. During angiogenesis, endothelial cells migrate through a 3D extracellular matrix (ECM) network that is rich in collagen. Migration efficiency and the mode of migration (e.g. the extent of integrin-dependency and the requirement of matrix metalloproteases) are determined by ECM properties including ligand density, stiffness, fiber crosslinking, and pore size [6–8]. These ECM properties are typically altered in tumor areas, e.g. ECM stiffening has been observed in tumor tissue [9, 10].

The ECM network may control angiogenesis in several ways. First, it acts as an organizing platform for growth factor distribution, activation, and presentation [11]. In vitro assays have shown that tissue deformation can regulate angiogenesis through spatial organization of activity of the VEGF pathway [12]. In addition, cells receive mechanical cues from the ECM through integrin-based cell-matrix adhesions [13–15]. In vivo studies have demonstrated that angiogenesis is an integral response to chemical and mechanical cues [16].

Here we use sequential microprinting of tumor and microvascular endothelial cells to investigate their mechanical interaction through ECM scaffolds. We use quantitative reflection microscopy analysis to study tumor-induced collagen orientation. We show that tumor spheroids can orient a collagen network to a distance of up to 5 times the tumor radius - far beyond the area of tumor expansion and cell migration. Furthermore, we demonstrate that microvascular endothelial cells sense and respond to such orientation provided that the oriented ECM is physically connected to the tumor spheroid. Together, our data indicates that ECM network reorientation acts as a remote mechanical cue to steer angiogenesis.

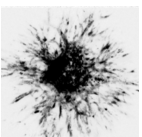
## 2.2 Results

### 2.2.1 Tumor spheroids in 3D collagen induce the reorientation of surrounding collagen

4T1 breast cancer spheroids were microprinted in collagen gels (Figure 2.1A) and their outgrowth and migration was monitored after 48 hours (Figure 2.1B). A spheroid mask was generated to define the final spheroid area including core spheroid and migrated cells (Figure 2.1C). Reflection microscopy was performed to analyze the collagen network surrounding this final spheroid area (Figure 2.1D). In 2 days the tumor spheroid radius (including core and migrated cells) had increased  $\sim 4$ -fold (Figure 2.1A,B). Concomitantly, reflection microscopy showed that the surrounding collagen network contained an increase in radially oriented fibers (Figure 2.1D, 2.2A). Indeed, quantitative image analysis showed an increase in collagen fibers with an orientation parameter  $\sim 1$  (dark red; denoting collagen directed radially towards the tumor spheroid center) close to the spheroid boundary (Figure 2.2A). By contrast, in areas distant from the spheroid, the number of fibers with an orientation parameter  $\sim 1$  equaled the number of fibers with an orientation parameter  $\sim 0$  (dark blue; denoting collagen oriented tangential to the tumor spheroid radius) (Figure 2.2A). Quantification of collagen fiber orientation throughout the gel relative to the distance from the final tumor spheroid edge (dashed red circle in Figure 2.1C,D) indicated that tumor spheroids that expanded from an average radius of  $116 \pm 21 \mu\text{m}$  to  $527 \pm 54 \mu\text{m}$  had caused radial orientation of collagen fibers up to 2.65 mm from the spheroid edge (i.e. 95% confidence interval  $> 0.5$  indicating orientation was significantly different from random) (Figure 2.2B). Thus, tumor spheroids induced remote orientation of collagen fibers up to distances of 5 times the spheroid radius.

### 2.2.2 Remote tumor-induced collagen network reorientation correlates with local cell migration capacity and requires Rho kinase-myosin activity

To address the role of collagen-binding integrins (mainly  $\alpha 1\beta 1$ ,  $\alpha 2\beta 1$ ) in tumor-induced collagen orientation we made use of cells stably expressing shRNAs targeting ITGB1, which express strongly reduced ( $\sim 90\%$ ) levels of  $\beta 1$  integrins [17]. For 4T1 cells, depletion of  $\beta 1$  integrins reduced



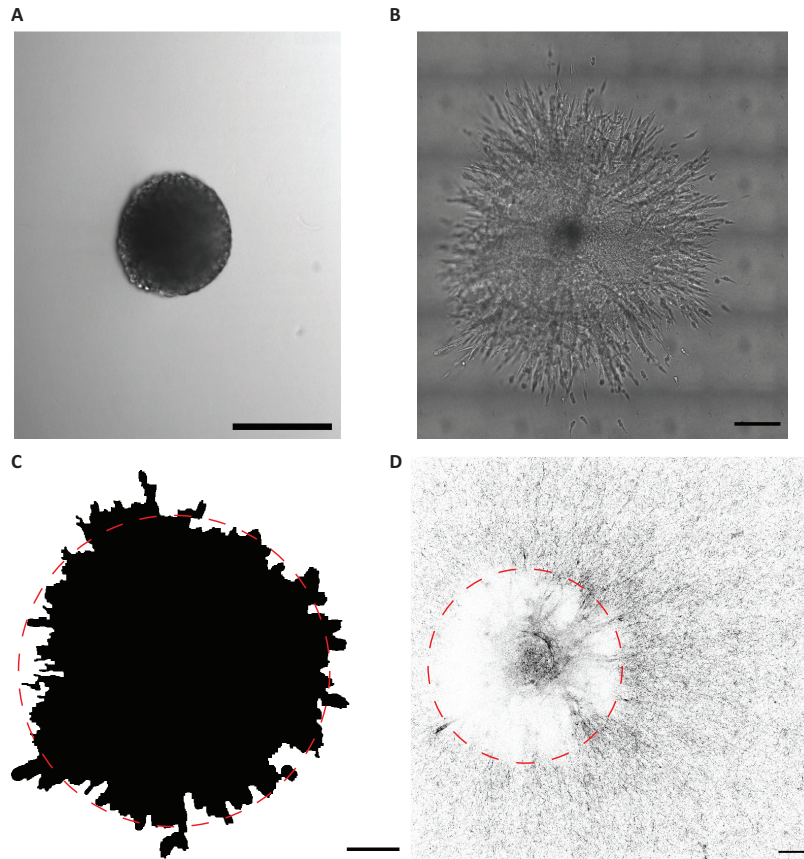


**Figure 2.1**

**4T1 breast cancer spheroid expansion and collagen network organization.** (A-B) 4T1 tumor spheroid at the day of injection (A) and 48 hours after injection (B). (C) Spheroid mask covering core spheroid and migrating cells at 48 hours, which was used as boundary for collagen organization calculations (red dashed circle). (D) Inverted reflection microscopy image with tumor border marked with red dashed circle, showing radial orientation of surrounding collagen. Scale bar, 200  $\mu\text{m}$ .

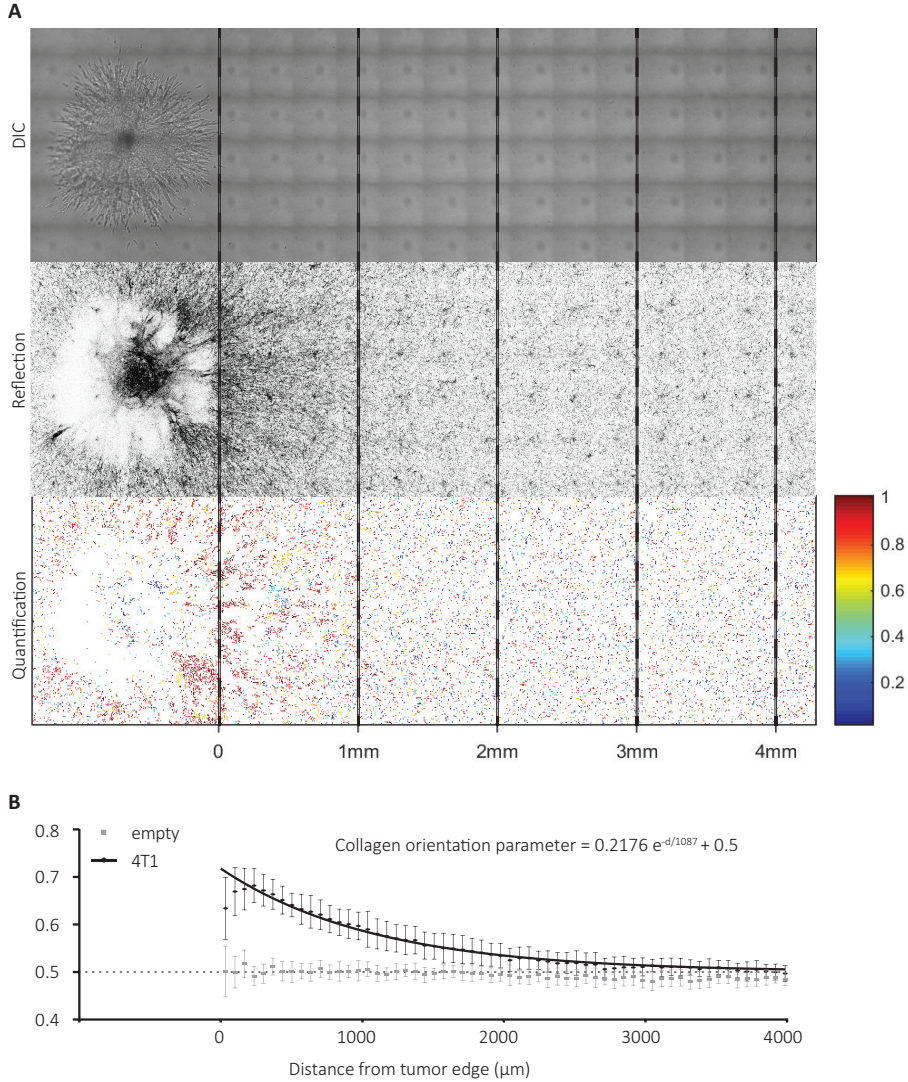
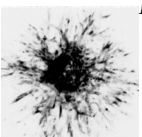


**Figure 2.2**

**4T1 breast cancer spheroids cause long distance radial orientation of surrounding collagen.** (A) Brightfield (top) and reflection microscopy (middle) images of collagen-embedded spheroid 48 hours post injection and corresponding collagen orientation detection (bottom). Red, radially oriented collagen fibers; blue, tangential collagen fibers. Dashed lines note the indicated distances from tumor spheroid border. Note the dense red at distance 0-1mm with gradually increasing randomness of colors at increasing distances. (B) Collagen orientation parameter calculated 48 hours after injection at the indicated distances from individual tumor spheroid borders for 29 4T1 injections (black circles) and 22 empty wells (gray squares) from 5 independent experimental replicas with standard deviations. The fit equation (black line) is shown.



spheroid expansion through collective migration and induced migration of individual cells, as described before [17] (Figure 2.3A). This was accompanied by reduced collagen orientation (measured beyond the area of spheroid expansion - cell migration) (Figure 2.3B). Similar results were obtained for HCC70-derived tumor spheroids (Figure S1A,B). By contrast, control MDA-MB-468 and BT20 tumor spheroids showed little migration whereas depletion of  $\beta 1$  integrins in these cells enhanced spheroid expansion through a mix of collective and single cell migration (Figure 2.3C and S1C). In these cases, depletion of  $\beta 1$  integrins led to an increased remote collagen orientation (Figure 2.3D and S1D). Lastly, in HCC1806 cells  $\beta 1$  integrin depletion caused a shift from relatively ineffective collective migration to similarly weak single cell migration and this did not affect the capacity of the tumor spheroids to cause collagen orientation (Figure 2.3E,F). Together, these results indicated that the capacity of tumor cells to orient the collagen network was not affected by a reduction in collagen-binding integrins per se. Rather, changes in integrin expression caused decreased or increased tumor cell migration at the spheroid edge, which correlated with decreased or increased remote collagen orientation capacity, respectively.

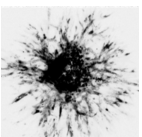
We next tested a larger panel of carcinoma and sarcoma cell lines for their capacity to orient surrounding collagen (Figure S2). In line with the results obtained with 4T1 cells, irrespective of the origin of the cell line,  $\beta 1$  integrin expression level, or migration strategy; there was a strong correlation between remote collagen orientation capacity and spheroid expansion (average initial spheroid radius for all cell lines was  $113 \pm 29$   $\mu\text{m}$ ) (Figure 2.4A,B). Spheroid expansion as measured included spheroid growth and migration and tumor cell types showing the largest spheroid expansions typically displayed strong migration activity. To investigate the role of cytoskeletal contractility, pharmacological inhibition of myosin II or Rho kinase that acts upstream of myosin II activity was used for the duration of the experiment. Treatment of 4T1 spheroids with a myosin II inhibitor caused a  $\sim 15\%$  decrease in final spheroid radius and reduced collective migration activity that was accompanied by a 50% reduction in remote collagen orientation (Figure 2.4C,D and S3). Inhibition of Rho kinase led to a  $\sim 8\%$  decrease in final spheroid radius and caused a switch from collective migration to individual cell migration that was accompanied by a 70% reduction in remote collagen orientation (Figure 2.4C,D and S3). These results showed that inhibition of Rho kinase-

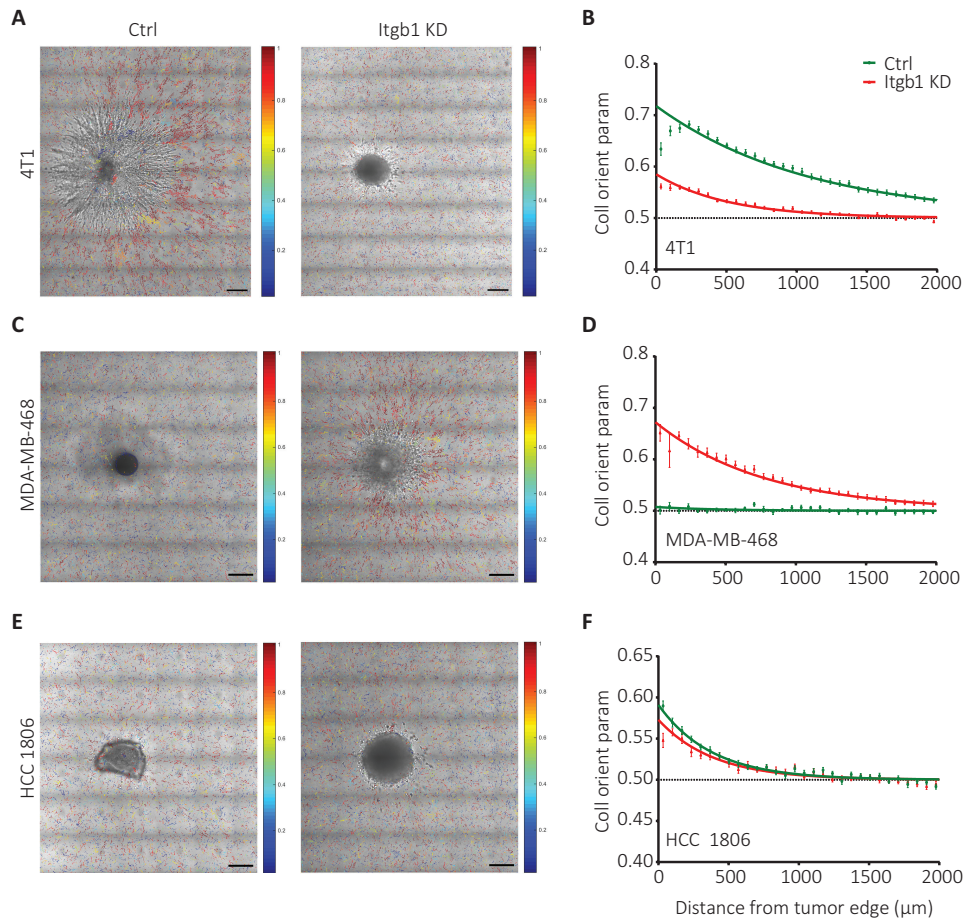
myosin II-mediated contractility has moderate effects on cell migration at the spheroid edge but strongly attenuates remote collagen orientation.

### 2.2.3 Endothelial spheroids orient in response to tumor-oriented collagen network

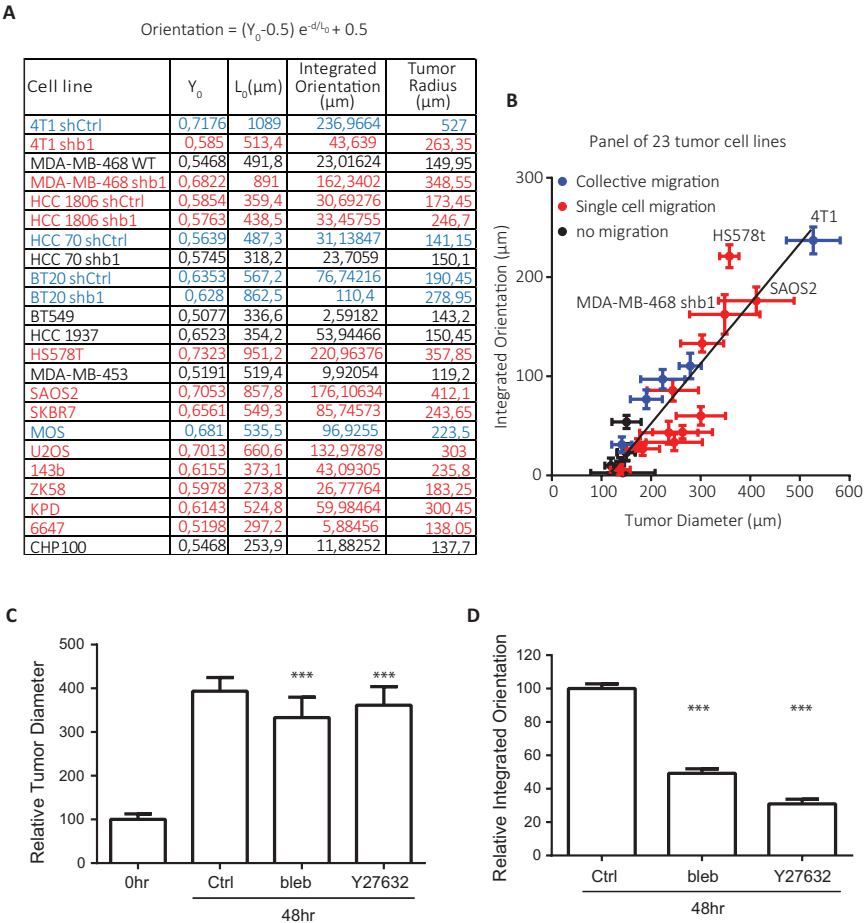
HMEC-1 human microvascular endothelial cells were injected at various defined x-y distances from 4T1 spheroids at 48 hours post 4T1 injection (Figure 2.5A and S4). The resulting endothelial spheroids were monitored by DIC 24 hours later and the direction of the tumor spheroid was marked (red arrow head) (Figure 2.5B). Endothelial spheroid masks were generated to study the orientation of their long axis (Figure 2.5C; blue arrows) and relate this to the relative position of the tumor spheroid (Figure 2.5C; red arrows). Alignment of the endothelial spheroid in the direction of the tumor spheroid was observed for injections within the 2.65mm collagen orientation area whereas this was lost for endothelial cells injected beyond this zone (Figure 2.5D).

Next, HMEC-1 cells were injected at varying distances from tumor spheroids derived from the panel of cell lines described above (Figure 2.6A). In accordance with the large variation in collagen orientation distance among these lines (Figure 2.4), the distance to which HMEC-1 cells could sense and respond to these spheroids differed strongly. Across the panel of cell lines, HMEC-1 spheroids present within a zone of strong tumor-oriented collagen were directed towards the tumor spheroid whereas direction of HMEC-1 spheroids was random if they were outside of this zone (Figure 2.6B-D). HMEC-1 directionality was induced in response to collagen orientation significantly above average as measured for all tested HMEC-1 injection coordinates (Figure 2.6B). This level of orientation was reached by 4T1, HCC70, Hs578t, SAOS2, U20S, MOS and KPD but not BT20 or MDA-MB-468 cells. In accordance with data shown above (Figure 2.3; S1)  $\beta 1$  integrin-depletion reduced above-threshold collagen orientation measurements for 4T1 and HCC 70 cells whereas this was induced for BT20 and MDA-MB-468 cells in response to ITGB1 silencing. Likewise, HMEC-1 spheroid elongation correlated with tumor-induced collagen orientation (Figure 2.6E,F) and combining HMEC-1 spheroid direction and elongation parameters showed a strong and significant HMEC orientation response to tumor-oriented collagen (Figure 2.6G,H).

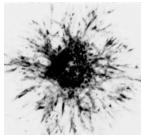


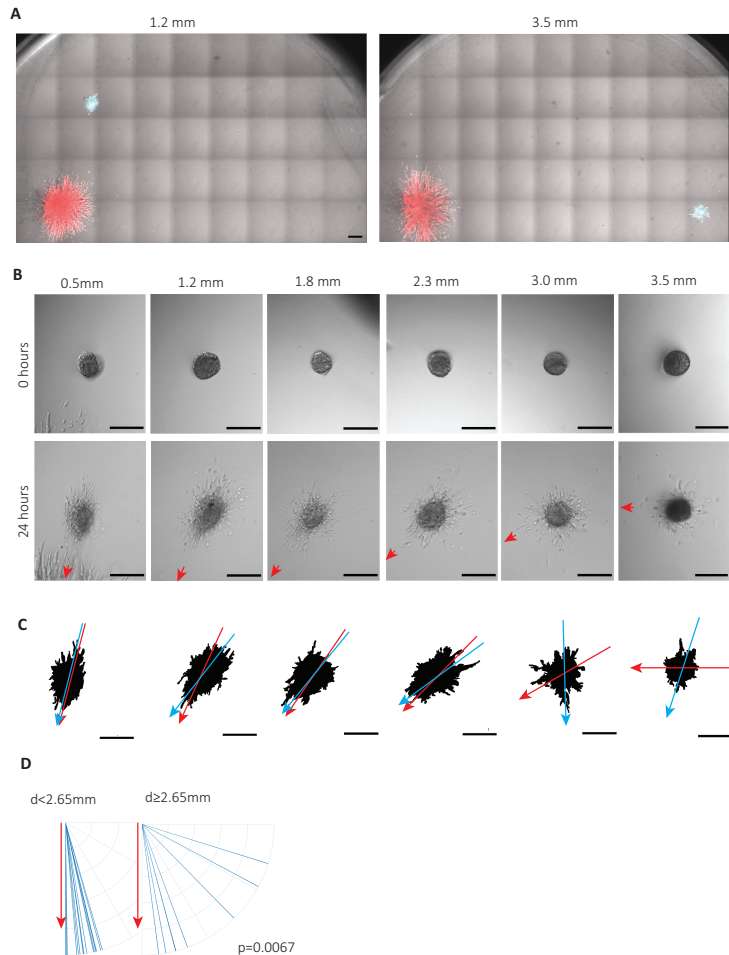
**Figure 2.3**

**Distinct effects of  $\beta 1$  integrin downregulation on tumor spheroid cell migration and collagen orientation.** (A,C,E) Collagen orientation images merged with brightfield images taken 48 hours after injecting the indicated cell lines with or without shRNA targeting ITGB1. (B,D,F) Collagen orientation measured at a range of distances from tumor border for 4T1 shctrl (B, green;  $n=29$ ), 4T1 shITGB1 (B, red;  $n=29$ ), MDA-MB-468 WT (D, green;  $n=16$ ), MDA-MB-468 shITGB1 (D, red;  $n=21$ ), HCC 1806 shctrl (F, green;  $n=20$ ), and HCC 1806 shITGB1 (F, red;  $n=21$ ) tumor spheroids 48 hours after injection mean  $\pm$  standard deviation with exponential fits (solid lines) from at least four independent experimental replicas is shown. Scale bar, 200  $\mu\text{m}$ .



**Figure 2.4**  
**Tumor induced collagen orientation and tumor expansion are interrelated and depend on ROCK-myosin II-induced contractility.** (A) Table showing the fit parameters  $Y_0$  and  $L_0$ , the area under the fitted curve (integrated orientation) and the tumor radius 48 hours after injection for indicated cell lines. (B) Graph showing relation between tumor radius at 48 hours post injection and integrated collagen orientation parameter for cell lines depicted in table A with distinct modes of migration as indicated based on DIC images. Plot shows mean, standard deviation and linear fit ( $Y=0.605(\pm 0.06)X-68.65(\pm 15.6)$ ;  $R^2=0.8251$ ). (C,D) Bar graphs showing mean and standard deviation of relative 4T1 tumor radius normalized to tumor size at 0hr (C), and relative integrated collagen orientation at 48 hours normalized to control (D) for no treatment (Ctrl;  $n=55$ ), 10  $\mu\text{M}$  blebbistatin (bleb;  $n=53$ ) and 10  $\mu\text{M}$  Y27632 (Y27632;  $n=46$ ). Combined data from three independent experiments is shown. \*\*\*;  $p<0.0005$  according to Mann-Whitney test (C) or unpaired t-test (D) compared to control at 48 hours.



**Figure 2.5**

**HMEC-1 microvascular endothelial cells injected within 4T1 remote area of oriented collagen show directional migration towards tumor spheroid.**

(A) Merged brightfield/fluorescence images taken at  $t=72$  hours showing CellTracker green CMFDA-labeled HMEC-1 cells injected at  $t=48$  hours at the indicated distances from the spheroid border of CellTracker Orange CMRA-labeled 4T1 cells injected at  $t=0$  hours. (B) Representative DIC images of HMEC-1 spheroids at the day of injection (top) or 24 hours after injection (bottom) at indicated distances from 4T1 tumor spheroids. The red arrows point towards the center of 4T1 tumor spheroid. (C) HMEC-1 spheroid masks generated for images shown in B (bottom). Blue arrow indicates major axis of the mask; red arrow points to 4T1 tumor spheroid center. (D) Major axis orientation of HMEC-1 spheroids (blue lines) injected at distances from 4T1 spheroid edge less ( $n=15$ ; left) or more than 2.65 mm ( $n=8$ ; right) plotted against the direction of the 4T1 tumor spheroid (set vertically for each experiment; red arrow). Data obtained from four independent experiments;  $P$  value calculated using Mann-Whitney test; scale bar, 200  $\mu\text{m}$ .

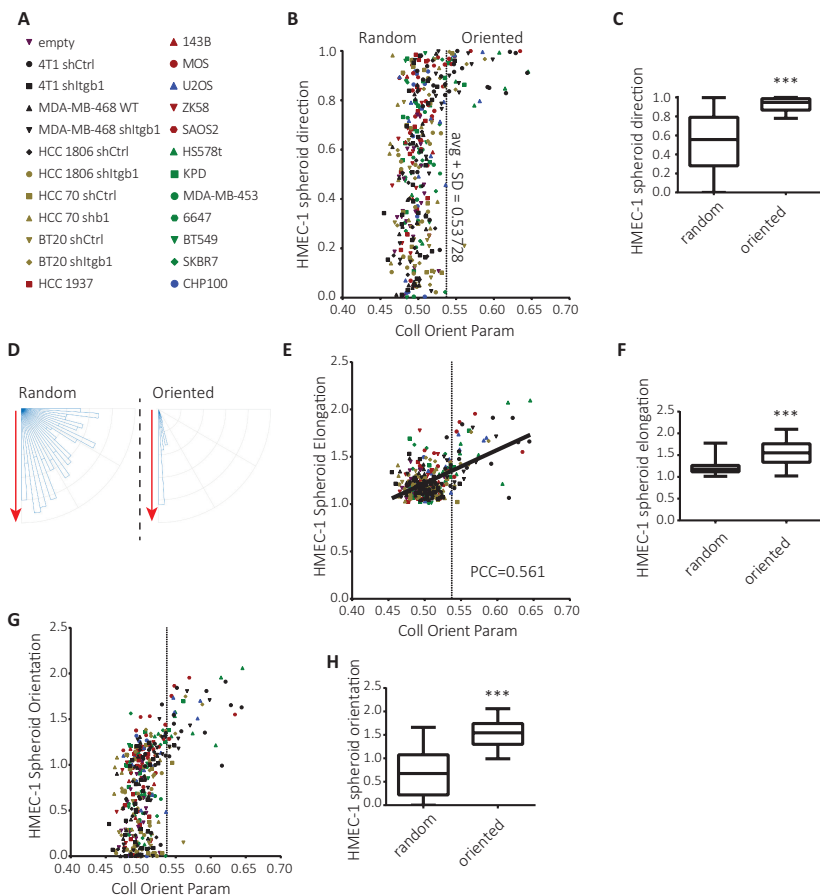
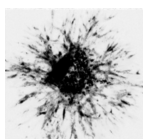


**Figure 2.6**

**Directional HMEC-1 migration towards tumor spheroid when injected within area of tumor-oriented collagen for panel of tumor cell lines.** (A) Panel of cell lines used with corresponding symbols. (B, E, G) Direction (B), elongation (E) and orientation (G) of HMEC-1 spheroids measured 24 hours after HMEC-1 injection at varying distances from panel of tumor spheroids (A) plotted against collagen orientation parameter at the corresponding distances (obtained in each case from reflection microscopy 48 hours after tumor cell injection just prior to HMEC-1 injection). Dashed line is drawn at one standard deviation above average collagen orientation parameter and indicates the threshold for "oriented collagen". (C, F, H) Box whisker graphs showing the minimum to maximum of direction (C), elongation (F) and orientation (H) of HMEC-1 spheroids injected in regions of oriented collagen vs regions of random collagen. (D) Major axis direction of HMEC-1 injections in oriented collagen vs random collagen plotted against the direction of the tumor spheroids (set vertically for each experiment; red arrow). \*\*\*,  $p < 0.0005$  according to Mann-Whitney test. PCC: calculated Pearson product-moment correlation coefficient.



### 2.2.4 Endothelial response to oriented collagen network requires physical coupling with tumor

To address if physical connections between the tumor spheroid and the oriented collagen network remained important for guidance of endothelial cells, the spheroid was physically disconnected after the collagen network had been oriented. For this purpose, two HMEC-1 spheroids were injected at the same distance from the tumor spheroid at opposite sides and laser cutting of collagen fibers was applied close to the tumor edge, between the tumor and one of the HMEC-1 spheroids (Figure 2.7A). Orientation of the collagen network was maintained in areas disconnected from the tumor spheroid through laser ablation (Figure 2.7B,C). However, HMEC-1 cells injected in such areas no longer responded to collagen orientation: HMEC-1 spheroid direction, elongation, and the combined orientation parameter were decreased; resembling HMEC-1 behavior in non-oriented collagen areas (Figure 2.7D-F). Control HMEC-1 spheroids in the same well that were still connected to the tumor normally responded to oriented collagen. These findings demonstrate that an intact physical connection of the oriented ECM network with the tumor spheroid is required for orientation sensing by the endothelial cells.

## 2.3 Discussion

The tumor stroma plays an important role in initiation and progression of cancer [18]. Mechanical properties of the ECM can influence tumor cell behavior and have been linked to prognosis. ECM stiffness [19–21], pore size [22–24], crosslinking [25], fiber alignment [26, 27], as well as the presence of stromal contractile cells [28] have all been shown to influence aspects of cancer progression, including tumor growth and invasion. Vice-versa, tumor cells actively modify these ECM properties thereby promoting tumor growth, invasion, and metastasis potential [29–32].

Here, we use quantitative reflection microscopy analysis to study remote tumor-mediated collagen network orientation. We show that tumor spheroids reorient a surrounding collagen-based ECM network up to five times their radius. In a panel of cell lines the distance of collagen orientation correlates with spheroid expansion which is mainly caused by tumor invasion/migration. Such long range collagen reorganization has also been observed for mouse fibroblast explants [33]. Local ECM reorga-

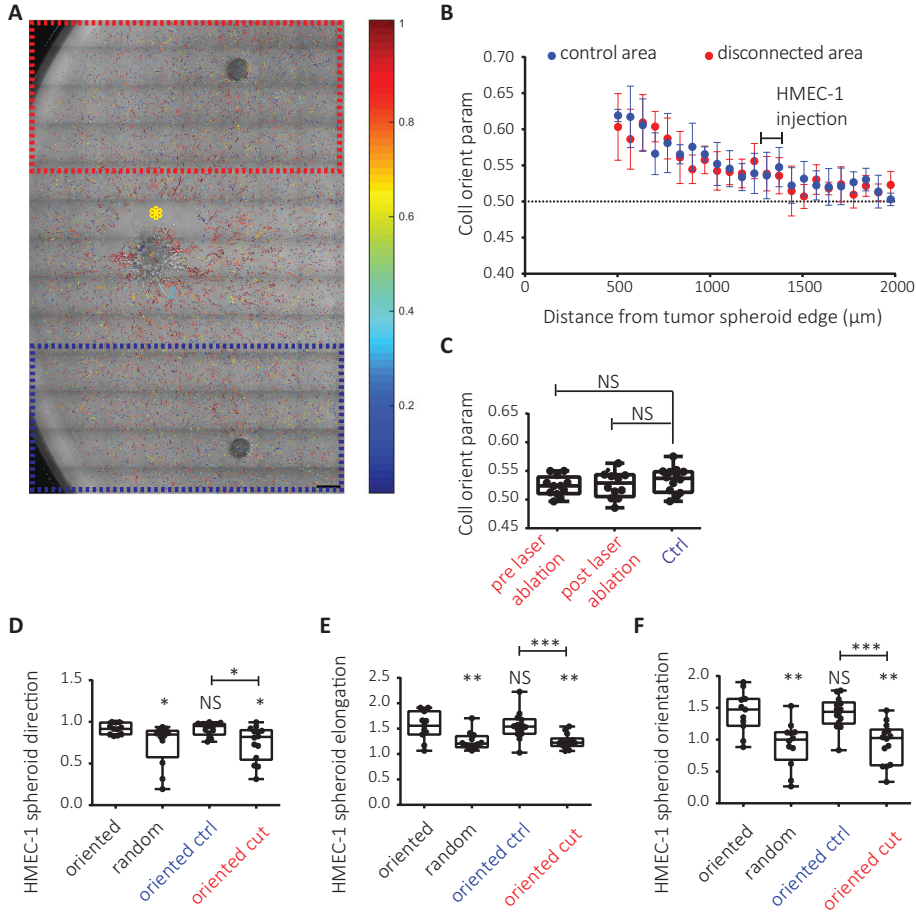
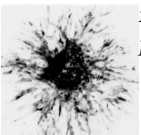


**Figure 2.7**

**Endothelial response to tumor-oriented collagen network depends on physical connection of oriented collagen network with the tumor.** (A) Collagen orientation image superimposed on brightfield image showing 4T1 spheroid (left center) and two HMEC-1 spheroids at the top and bottom of the image at ~1.4mm from the 4T1 injection. Yellow asterisk indicates area of laser ablation 48 hours post 4T1 injection just after HMEC-1 injection; red box, area disconnected from the tumor; blue box, control area. (B) Collagen orientation parameter (mean  $\pm$  standard deviation) for control (blue) and disconnected (red) areas shown in (A) with HMEC-1 injections performed at the indicated region. (C) Box whisker graphs showing the minimum to maximum of collagen orientation parameter at HMEC-1 injection sites just prior to HMEC-1 injection for blue box in Figure A (Ctrl) and red box in Figure A before and after laser ablation. (D-F) Box whisker graphs showing the minimum to maximum of direction (D), elongation (E) and orientation (F) of HMEC-1 spheroids injected in oriented or random collagen regions (black legends; data for 4T1 cells from Figure 5) or injected in the blue box (oriented ctrl) or the disconnected red box (oriented cut) as indicated in A. NS,  $p > 0.05$ ; \*,  $p < 0.05$ ; \*\*,  $p < 0.01$ ; \*\*\*,  $p < 0.001$  relative to oriented unless otherwise indicated; Mann-Whitney test; Scale bar, 200  $\mu\text{m}$ .



nization in areas containing tumor cells is driven by Rho kinase-Myosin II-mediated contractility [20, 34, 35]. Our findings indicate that traction forces applied by the tumor cells on the local collagen network drives ECM reorientation also in distant areas where tumor cells are absent. In fact, while consequences of contractility inhibition for local tumor cell migration are limited, which can be explained by tumor cell plasticity, remote ECM reorientation is strongly attenuated.

Antibody blocking experiments have shown that collagen-binding integrins mediate i) local tumor-induced collagen network reorganization [36], and ii) tumor cell-responses to mechanical ECM properties [25]. Gene silencing as used in our study may be less efficient than antibody blocking. Nevertheless, we observe highly distinct effects of  $\beta 1$  integrin silencing on collagen network reorientation. We and others have previously shown that depletion or blockade of  $\beta 1$  integrins can either inhibit migration or cause a switch from collective to single cell migration, e.g. through effects on TGF- $\beta$  signaling [17, 37, 38]. Our current study shows that in tumors where collective migration is attenuated or switched to less abundant individual cell migration in response to  $\beta 1$  integrin silencing, collagen network reorientation is lost (e.g. 4T1); whereas in tumors where cell motility is normally very poor and  $\beta 1$  integrin silencing triggers more abundant (individual) cell migration, a concomitant increase in collagen network reorientation is observed (e.g. MDA-MB-468). The fact that  $\beta 1$  integrin silencing does not directly attenuate collagen organization may point to roles for other collagen-binding receptors. On stromal fibroblasts, syndecan-1 participates in ECM network alignment [39]. Likewise, syndecans or discoidin domain collagen receptors on tumor cells may be candidates for force-induced collagen reorganization in the context of strongly reduced integrin levels.

The experiments discussed above show that tumor spheroids can reorient the collagen network at relatively long distances, way beyond the area of tumor expansion and migration. We subsequently show that endothelial cells can sense such long-range orientation and respond by moving towards the tumor. It is known that mechanical ECM properties, such as density and stiffness regulate angiogenesis [40–43]. This may be explained by changes in the distribution of soluble factors or enhanced activity of the receptors for these factors [12, 44, 45]. Alternatively, physical aspects of the network may instruct endothelial cell behavior. Indeed, we show that tumor-mediated remote radial organi-

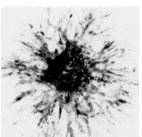
zation of collagen directs human microvascular endothelial cells. The correlation between levels of remote collagen organization and induction of endothelial cell directionality holds through for a panel of  $\sim 20$  different human cancer cell lines. Importantly, laser ablation of collagen fibers close to the tumor does not affect the architecture of the remote collagen network but leads to complete loss of endothelial cell responsiveness to such oriented ECM regions. This argues against a mechanism involving chemotactic signals. It also indicates that contact guidance, i.e. a preference for aligned collagen fibers, is insufficient. Rather, once the collagen network is organized, distant forces applied to the network by the tumor are critical for sensing and/or responding of endothelial cells.

Taken together, our study shows for the first time that a radial collagen network organization generated by the tumor relatively far beyond the area of tumor expansion and migration, not only forms migratory highways for tumor invasion but can also guide angiogenesis in a manner dependent on tumor generated traction forces. In coordination with soluble factors, this mechanical interaction might further direct microvascular sprouts towards the tumor. Hence, targeting tumor induced ECM remodeling may prevent both tumor invasion and angiogenesis.

## 2.4 Materials and methods

### 2.4.1 Cell culture

4T1 mouse breast cancer cells and BT20, BT549, HCC1806, HCC1937, HCC70, HS578t, MDA-MB-453, MDA-MB-468, and SKBR7 human breast cancer cells purchased from the American Type Culture Collection or provided by Dr. J Foekens, Erasmus Medical Center, Rotterdam NL [46] were grown in RPMI1640 medium supplemented with 10% fetal bovine serum (GIBCO, USA), 25 U/ml penicillin and 25  $\mu\text{g}/\text{ml}$  streptomycin (Invitrogen). Human osteosarcoma cell lines MOS, U2OS, 143B, ZK58, SAOS2, and KPD were described previously [47] and grown in the same medium. Human Ewing sarcoma cell lines 6647 and CHP100 were provided by Dr. P. Hogendoorn, Leiden University Medical Center, Leiden NL, and maintained in IMDM cell culture medium (GIBCO) supplemented with 10% fetal bovine serum, 25 U/ml penicillin and 25  $\mu\text{g}/\text{ml}$  streptomycin. Stable bulk-sorted ITGB1-silenced tumor cell lines were described previously [17]. HMEC-1 human microvascular endothelial cells [48] were cultured in MCDB131 medium (GIBCO) supplemented



with 15% fetal bovine serum, 200 mM L-Glutamine, 10  $\mu\text{g}/\text{mL}$  epidermal growth factor, 100  $\mu\text{g}/\text{mL}$  hydrocortisone, 25 U/ml penicillin and 25  $\mu\text{g}/\text{ml}$  streptomycin. All cells were cultured in a humidified incubator at 37°C with 5%  $\text{CO}_2$ .

### 2.4.2 Automated sequential microprinting of tumor- and endothelial cells in ECM scaffolds

Collagen type I solution was isolated from rat-tail collagen by acid extraction as described previously [49]. Collagen was diluted to 1 mg/mL in the culture medium containing 0.1 M Hepes (BioSolve) and fixed to pH 7.5 by addition of  $\text{NaHCO}_3$  (stock 440 mM, Merck). 60  $\mu\text{L}$  of this solution was then pipetted into a glass-bottom 96 well plate (Greiner) and incubated for 1 hour at 37°C to polymerize.

Automated injection of cell suspensions into the resulting collagen gels to generate arrays of cell spheroids with defined x-y-z position was performed as described using injection robotics from Life Science Methods, Leiden NL (<http://www.lifesciencemethods.com>) [17, 50]. Tumor spheroids of  $113 \pm 29$   $\mu\text{m}$  initial radius were generated at 200  $\mu\text{m}$  above the glass surface (average collagen gel height  $\sim 1.5$  mm) and incubated 48 hours with appropriate culture media for each cell line. Subsequently, medium was removed, HMEC-1 cells were injected at the same z-position at various defined x-y distances from the tumor spheroid, and wells were further incubated with HMEC-1 culture media for 24 hours (Figure S4).

For experiments where tumor spheroids were treated with Myosin II or Rho kinase inhibitors, media was supplemented with blebbistatin (Calbiochem cat. number 203389, Merck KGaA, Darmstadt, Germany) or Y27632 (Tocris cat. number 1254, Bristol, UK), respectively reaching 10  $\mu\text{M}$  final concentration (medium+gel). For fluorescent imaging of 4T1 and HMEC-1, cells were incubated at 37°C with 1  $\mu\text{M}$  CellTracker Orange CMRA or CellTracker Green CMFDA Dye, respectively for 15 minutes prior to injection.

### 2.4.3 Collagen gel imaging

Spheroids were imaged using a Nikon TE2000 confocal microscope equipped with a Prior stage controlled by NIS Element Software and with a temperature and  $\text{CO}_2$ -controlled incubator. Frame stitching was used when necessary. Differential interference contrast (DIC) images were captured

using a charged coupled device (CCD) camera with NIS software and 10x dry objective. Reflection microscopy of the entire well was performed by 5.4 mm x 5.4 mm stitching of images obtained using a 40x long distance water immersion objective by illuminating with a 561 nm laser coupled with a 561 nm blocking dichroic mirror for the detection.

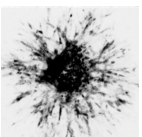
#### 2.4.4 Laser severing assay

After injecting HMEC-1 cells on both sides of the tumor spheroid at a distance of 1650  $\mu\text{m}$  from the tumor spheroid center, laser severing was performed by applying 16 lines/second stimulation just outside of the tumor spheroid with infrared laser (Coherent Chameleon Discovery) at 790 nm wavelength at full power ( $\sim 3000$  mW), using the 40x long distance water immersion lens, while manually scanning through the z plane over a duration of five minutes. This was repeated until all the collagen at one side of the tumor spheroid was cut.

#### 2.4.5 Image analysis

All image analysis was performed using in house written Matlab scripts (Mathworks, Natick, MA, USA). DIC images were first put through a median filter to create a background illumination signal to which the original images were normalized. Normalized images were blurred and a mask for core detection was generated by thresholding for signal lower than two standard deviations below the mean and taking only the central binary image. Subsequently, a canny edge detection method was applied to the normalized image to mask the outer rim of the spheroid. This mask was dilated to include the area of single cell migration and combined with the core mask to capture the entire final spheroid.

For reflection image analysis, first a background image was calculated by applying a circular averaging filter of 10 pixel radius to the original image. This image was then subtracted from the original image and a customized rollingball filter was applied to extract fibrillar structures. The filter multiplied the signal with itself and used a local thresholding algorithm assigning pixels with squared intensities  $>0.5$  standard deviations above mean squared intensity within 5px distance, to a collagen fiber. From this binary image, isolated pixels were removed, a binary closure was performed, and structures of  $>20$  pixels and eccentricity  $>0.9$  were assigned as fibers.



The directionality of a fiber was quantified by first manually determining the center of the tumor spheroid per image, and subsequently calculating for each fiber; the cosine square of the angle between the vector pointing from the tumor spheroid to the center of the collagen fiber and the orientation of the collagen fiber. The distance of a fiber to the tumor edge was calculated by subtracting the previously determined tumor spheroid radius (obtained from the DIC image analysis) from the distance of the fiber center to the tumor spheroid center. Fiber orientations were analyzed depending on their distance, in bins of 100px (67  $\mu\text{m}$ ). To this data a two-parameter single exponential plateauing at 0.5 was fitted with the equation  $Y=(p1-0.5)\exp(-X/p2)+0.5$  for  $x$  (distance) larger than 100  $\mu\text{m}$  using GraphPad Prism 6 program (GraphPad Software, La Jolla, CA). Integrated orientation was calculated from the fit by taking the integral  $\int_0^\infty (p1 - 0.5)\exp(-X/p2) dx$  which yielded the result  $(p1-0.5)*p2$ .

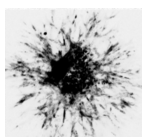
The collagen organization at the locations of HMEC-1 spheroids that were injected at designated distances from tumor center was determined by quantifying the collagen organization at that distance from the tumor spheroid before the HMEC-1 injections were performed, except when quantifying collagen orientation for the laser severing experiment for which the collagen organization was quantified both before HMEC-1 injection and after HMEC-1 injection/laser severing was performed. The HMEC-1 direction was determined by calculating the angle between the vector pointing from the HMEC-1 center to the tumor spheroid center and HMEC-1 long axis obtained from the injection mask, subtracting this angle from 90 degrees and dividing by 90 degrees so that HMEC-1 directed towards the tumor had a direction of 1 and directed perpendicularly had a direction 0. The elongation was calculated by dividing the long axis by the short axis length for the injection mask. Pearson product-moment correlation coefficient and linear fit were obtained using GraphPad Prism 6 software. The spheroid orientation was calculated by multiplying the direction with the elongation parameter.

To calculate significance between two conditions, the Mann-Whitney U test was used when comparing distribution data, and unpaired t-test was used when comparing integrated collagen orientation.

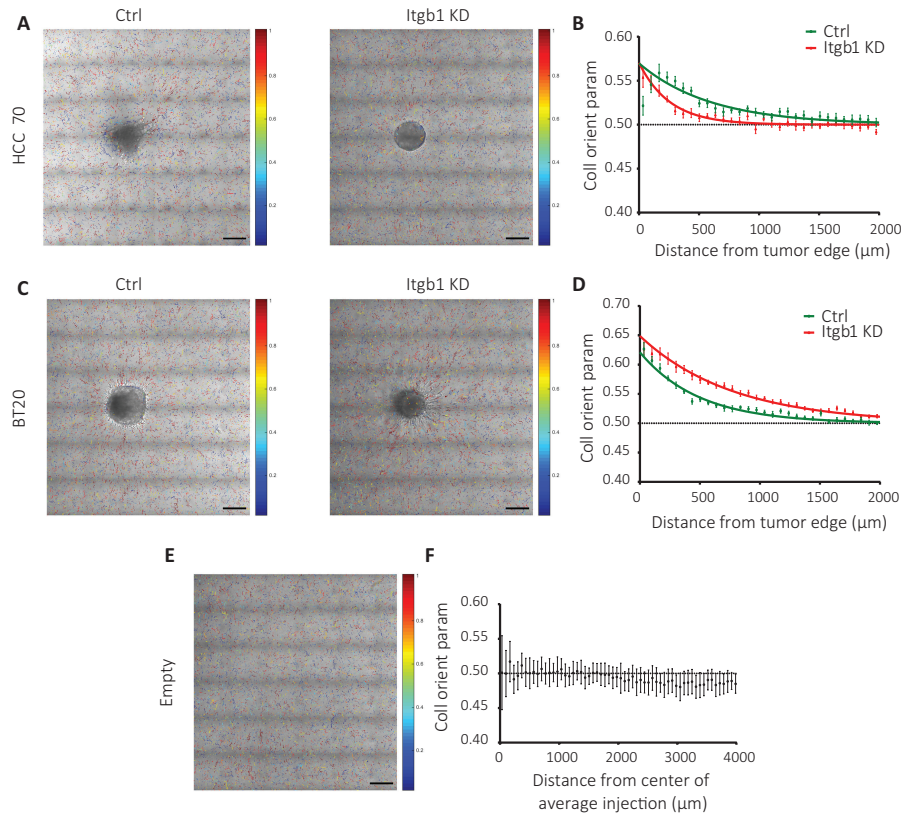
## 2.5 Acknowledgements

We thank Dr. Foekens and Dr. Hogendoorn for providing cell lines and Ms Tian Shu Fang (Division of Toxicology, Leiden Academic Center for Drug Research, Leiden, the Netherlands) for help setting up reflection microscopy technique.

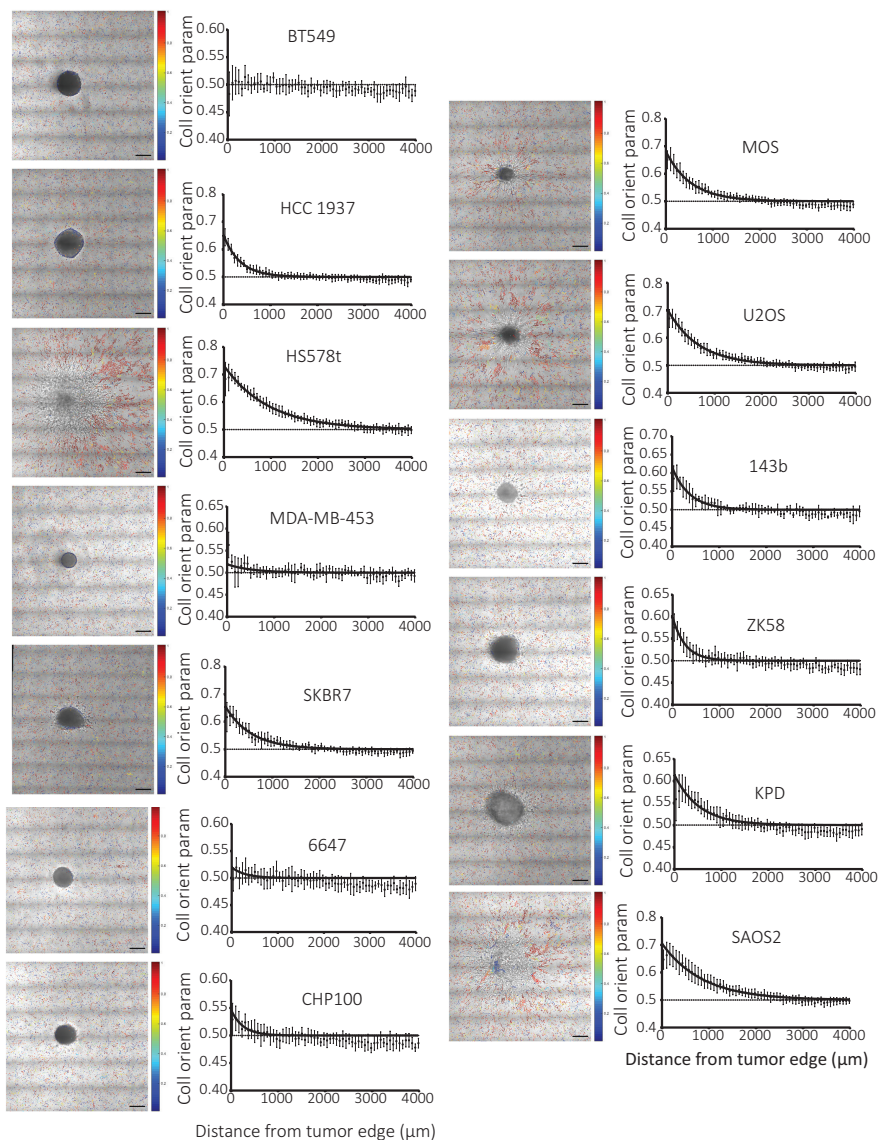
**Funding:** Support for this work came from the Netherlands Organization for Scientific Research (FOM 09MMC03). **Authors' contributions:** H.E.B. performed the experiments and analyzed the data. B.v.d.W. provided imaging infrastructure and critically read the manuscript. H.E.B. and E.H.J.D designed the experiments, interpreted data and wrote the manuscript. **Competing interests:** The authors declare no competing interests.



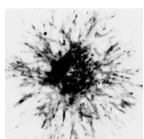
## 2.6 Supplemental figures

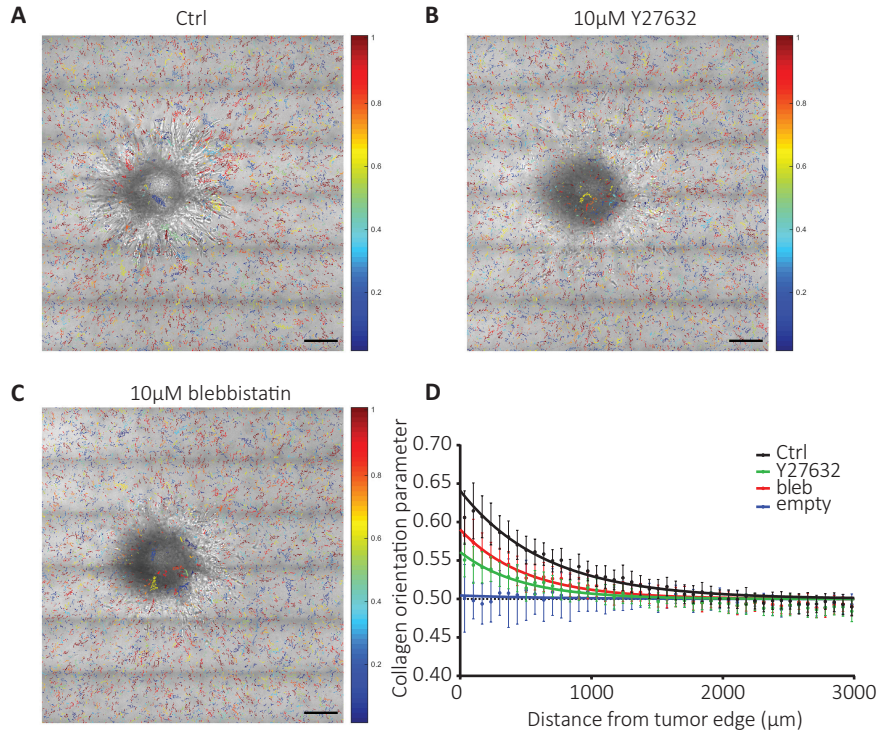
**Figure S1**

**Effects of  $\beta 1$  integrin downregulation on tumor spheroid cell migration and collagen orientation.** (A,C,E) Collagen orientation images merged with brightfield images taken 48 hours after injecting the indicated cell lines with or without shRNA targeting *ITGB1* (A,C) or without injection (E). (B,D,F) Collagen orientation measured at a range of distances from tumor border for HCC 70 shctrl (B, green;  $n=16$ ), HCC 70 shITGB1 (B, red;  $n=15$ ), BT20 shctrl (D, green;  $n=17$ ), BT20 shITGB1 (D, red;  $n=17$ ) tumor spheroids 48 hours after injection, and from the average injection location for empty well (F, black;  $n=22$ ) at the same time point, mean  $\pm$  standard deviation with exponential fits (solid lines) from at least three independent experimental replicas is shown. Scale bar, 200  $\mu\text{m}$ .

**Figure S2**

**Collagen organization and tumor expansion for a panel of cell lines.** Collagen orientation images merged with brightfield images (left) taken 48 hours after injecting the indicated human breast cancer and sarcoma cells and corresponding collagen orientation measured at a range of distances from tumor border (right), mean  $\pm$  standard deviation with exponential fits (solid lines) is shown. Scale bar, 200  $\mu$ m.



**Figure S3**

**Effect of Y27632 and blebbistatin treatment on collagen organization.** (A-C) Collagen orientation images merged with brightfield images of 4T1 spheroids grown 48 hours in absence (A) or presence of 10 μM Y27632 (B) or 10 μM blebbistatin (C). (D) Collagen orientation measured at a range of distances from spheroid border for 4T1 injections after 48 hours without treatment (black,  $n=55$ ), with 10 μM Y27632 (green,  $n=46$ ) or 10 μM blebbistatin treatment (red,  $n=53$ ) or from the average injection location for empty well (blue,  $n=23$ ) at the same time point, mean  $\pm$  standard deviation with exponential fits (solid lines) from three independent experimental replicas is shown. Scale bar, 200 μm.

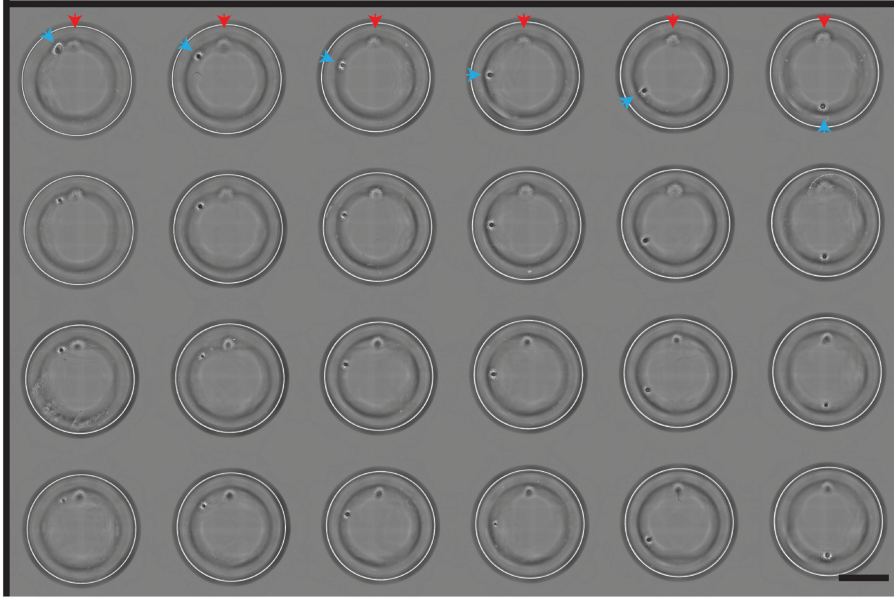
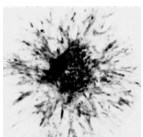


**Figure S4**

**Automated sequential microinjection layout for tumor spheroid-HMEC-1 interaction.** Low magnification image of multiwell plate showing 4T1 cells (red arrow heads) injected at identical x-y-z position in each well followed by HMEC-1 cells (blue arrow heads) injected at varying distances, 48 hours later and incubated for an additional 24 hours. Scale bar, 3mm.



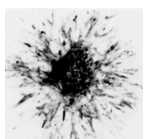
---

## BIBLIOGRAPHY

---

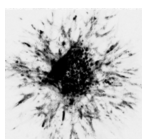
- [1] Judah Folkman. “Angiogenesis: an organizing principle for drug discovery?” In: *Nature Reviews Drug Discovery* 6.4 (2007).
- [2] Douglas Hanahan and Robert A Weinberg. “Hallmarks of cancer: the next generation”. In: *Cell* 144.5 (2011).
- [3] Peter Carmeliet and Rakesh K Jain. “Molecular mechanisms and clinical applications of angiogenesis”. In: *Nature* 473.7347 (2011).
- [4] Sara Weis and David A Cheresch. “Tumor angiogenesis: molecular pathways and therapeutic targets”. In: *Nature Medicine* 17.11 (2011).
- [5] M M Sholley et al. “Mechanisms of neovascularization. Vascular sprouting can occur without proliferation of endothelial cells”. In: *Laboratory Investigation* 51.6 (1984).
- [6] Peter Friedl et al. “New dimensions in cell migration”. In: *Nature Reviews. Molecular Cell Biology* 13.11 (2012).
- [7] Tim Lämmermann et al. “Rapid leukocyte migration by integrin-independent flowing and squeezing”. In: *Nature* 453.7191 (2008).
- [8] Katarina Wolf et al. “Physical limits of cell migration: Control by ECM space and nuclear deformation and tuning by proteolysis and traction force”. In: *The Journal of Cell Biology* 201.7 (2013).
- [9] Laura Kass et al. “Mammary epithelial cell: Influence of extracellular matrix composition and organization during development and tumorigenesis”. In: *The International Journal of Biochemistry & Cell Biology* 39.11 (2007).
- [10] Michael W Pickup, Janna K Mouw, and Valerie M Weaver. “The extracellular matrix modulates the hallmarks of cancer”. In: *EMBO Reports* 15.12 (2014).

- [11] Richard O Hynes. “The extracellular matrix: Not just pretty fibrils”. In: *Science (New York, N.Y.)* 326.5957 (2009).
- [12] Nicolas C Rivron et al. “Tissue deformation spatially modulates VEGF signaling and angiogenesis”. In: *Proceedings of the National Academy of Sciences of the United States of America* 109.18 (2012).
- [13] Hayri E Balcioglu et al. “Integrin expression profile modulates orientation and dynamics of force transmission at cell matrix adhesions”. In: *Journal of Cell Science* (2015).
- [14] Frederick Grinnell and Matthew W Petroll. “Cell motility and mechanics in three-dimensional collagen matrices”. In: *Annual Review of Cell and Developmental Biology* 26 (2010).
- [15] Pere Roca-Cusachs, Thomas Iskratsch, and Michael P Sheetz. “Finding the weakest link - exploring integrin-mediated mechanical molecular pathways”. In: *Journal of Cell Science* 125.13 (2012).
- [16] Akiko Mammoto et al. “A mechanosensitive transcriptional mechanism that controls angiogenesis”. In: *Nature* 457.7233 (2009).
- [17] Hoa H Truong et al. “ $\beta 1$  integrin inhibition elicits a prometastatic switch through the TGF $\beta$ -miR-200-ZEB network in E-cadherin-positive triple-negative breast cancer”. In: *Science Signaling* 7.312 (2014).
- [18] Pengfei Lu, Valerie M Weaver, and Zena Werb. “The extracellular matrix: A dynamic niche in cancer progression”. In: *Journal of Cell Biology* 196.4 (2012).
- [19] Ovijit Chaudhuri et al. “Extracellular matrix stiffness and composition jointly regulate the induction of malignant phenotypes in mammary epithelium”. In: *Nature Materials* 13.10 (2014).
- [20] Matthew J Paszek et al. “Tensional homeostasis and the malignant phenotype”. In: *Cancer Cell* 8.3 (2005).
- [21] Robert W Tilghman et al. “Matrix Rigidity Regulates Cancer Cell Growth by Modulating Cellular Metabolism and Protein Synthesis”. In: *PLoS One* 7.5 (2012).
- [22] Shawn P Carey et al. “Biophysical control of invasive tumor cell behavior by extracellular matrix microarchitecture”. In: *Biomaterials* 33.16 (2012).



- [23] Asja Guzman, Michelle J Ziperstein, and Laura J Kaufman. “The effect of fibrillar matrix architecture on tumor cell invasion of physically challenging environments”. In: *Biomaterials* 35.25 (2014).
- [24] Jiranuwat Sapudom et al. “The phenotype of cancer cell invasion controlled by fibril diameter and pore size of 3D collagen networks”. In: *Biomaterials* 52 (2015).
- [25] Kandice R Levental et al. “Matrix Crosslinking Forces Tumor Progression by Enhancing Integrin Signaling”. In: *Cell* 139.5 (2009).
- [26] Matthew W Conklin et al. “Aligned collagen is a prognostic signature for survival in human breast carcinoma”. In: *The American Journal of Pathology* 178.3 (2011).
- [27] Kristin M Riching et al. “3D collagen alignment limits protrusions to enhance breast cancer cell persistence”. In: *Biophysical Journal* 107.11 (2014).
- [28] Shalini Menon and Karen A Beningo. “Cancer cell invasion is enhanced by applied mechanical stimulation”. In: *PLoS One* 6.2 (2011).
- [29] Dewi Harjanto, Joseph S Maffei, and Muhammad H Zaman. “Quantitative analysis of the effect of cancer invasiveness and collagen concentration on 3D matrix remodeling”. In: *PLoS One* 6.9 (2011).
- [30] Casey M Kraning-Rush, Joseph P Califano, and Cynthia A Reinhart-King. “Cellular traction stresses increase with increasing metastatic potential”. In: *PLoS One* 7.2 (2012).
- [31] Daniel J McGrail et al. “Actomyosin tension as a determinant of metastatic cancer mechanical tropism”. In: *Physical Biology* 12.2 (2015).
- [32] Michael S Samuel et al. “Actomyosin-Mediated Cellular Tension Drives Increased Tissue Stiffness and beta-Catenin Activation to Induce Epidermal Hyperplasia and Tumor Growth”. In: *Cancer Cell* 19.6 (2011).
- [33] David Stopak and Albert K. Harris. “Connective tissue morphogenesis by fibroblast traction”. In: *Developmental Biology* 90.2 (1982).

- [34] Paolo P Provenzano et al. "Contact Guidance Mediated Three-Dimensional Cell Migration is Regulated by Rho/ROCK-Dependent Matrix Reorganization". In: *Biophysical Journal* 95.11 (2008).
- [35] Jeffrey B Wyckoff et al. "ROCK- and myosin-dependent matrix deformation enables protease-independent tumor-cell invasion in vivo". In: *Current Biology* 16.15 (2006).
- [36] James A Schiro et al. "Integrin alpha 2 beta 1 (VLA-2) mediates reorganization and contraction of collagen matrices by human cells". In: *Cell* 67.2 (1991).
- [37] Yael Hegerfeldt et al. "Collective cell movement in primary melanoma explants: plasticity of cell-cell interaction, beta1-integrin function, and migration strategies". In: *Cancer Research* 62.7 (2002).
- [38] Jenny G Parvani et al. "Targeted inactivation of beta1 integrin induces beta3 integrin switching, which drives breast cancer metastasis by TGF-beta." In: *Molecular Biology of the Cell* 24.21 (2013).
- [39] Ning Yang et al. "Syndecan-1 in breast cancer stroma fibroblasts regulates extracellular matrix fiber organization and carcinoma cell motility". In: *The American Journal of Pathology* 178.1 (2011).
- [40] Daniel R Croft et al. "Conditional ROCK activation in vivo induces tumor cell dissemination and angiogenesis". In: *Cancer Research* 64.24 (2004).
- [41] Kaustabh Ghosh et al. "Tumor-derived endothelial cells exhibit aberrant Rho-mediated mechanosensing and abnormal angiogenesis in vitro". In: *Proceedings of the National Academy of Sciences of the United States of America* 105.32 (2008).
- [42] Brooke N Mason et al. "Tuning three-dimensional collagen matrix stiffness independently of collagen concentration modulates endothelial cell behavior". In: *Acta Biomaterialia* 9.1 (2013).
- [43] Amir Shamloo and Sarah C Heilshorn. "Matrix density mediates polarization and lumen formation of endothelial sprouts in VEGF gradients". In: *Lab on a Chip* 10.22 (2010).
- [44] Yinying Dong et al. "Increasing matrix stiffness upregulates vascular endothelial growth factor expression in hepatocellular carcinoma cells mediated by integrin  $\beta 1$ ". In: *Biochemical and Biophysical Research Communications* 444.3 (2014).



- [45] Jie Liu and Sudha Agarwal. “Mechanical signals activate vascular endothelial growth factor receptor-2 to upregulate endothelial cell proliferation during inflammation”. In: *The Journal of Immunology* 185.2 (2010).
- [46] Antoinette Hollestelle et al. “Distinct gene mutation profiles among luminal-type and basal-type breast cancer cell lines”. In: *Breast Cancer Research and Treatment* 121.1 (2010).
- [47] Zuzanna Baranski et al. “Aven-mediated checkpoint kinase control regulates proliferation and resistance to chemotherapy in conventional osteosarcoma”. In: *The Journal of Pathology* 236.3 (2015).
- [48] Edwin W Ades et al. “HMEC-1: Establishment of an immortalized human microvascular endothelial cell line”. In: *The Journal of Investigative Dermatology* 99.6 (1992).
- [49] Navneeta Rajan et al. “Preparation of ready-to-use, storable and reconstituted type I collagen from rat tail tendon for tissue engineering applications”. In: *Nature Protocols* 1.6 (2006).
- [50] Hoa H Truong et al. “Automated microinjection of cell-polymer suspensions in 3D ECM scaffolds for high-throughput quantitative cancer invasion screens”. In: *Biomaterials* 33.1 (2012).

